Jour. Geol. Soc. India (2022) 98:1301-1307
https://doi.org/10.1007/s12594-022-2166-z

ORIGINAL ARTICLE

# Processing of Multispectral ASTER Data to Delineate Bauxite Abundant Zones and its Geochemical Characterisation Deposited over Deccan Traps of Central India in Mainpat Plateau, Surguja District, Chhattisgarh

Sanjay Kumar Balabantaray[1,*], S. Aravindan[1], Taanya Baunthiyal[2], R. Ravi[1]

[1]Department of Earth Sciences, Annmalai University, Annamalainagar - 608 002, India
[2]Indian Institute of Remote Sensing (ISRO), Dehradun - 248 001, India
***E-mail:*** *sanjaybalabantaray3@gmail.com*; aravindan_rs@yahoo.com; taanigeo.iirs@gmail.com; rajuravi9725@gmail.com*

*Received: 21 January 2021 / Revised form Accepted: 4 June 2021*


## ABSTRACT

**The current study deals with the application of Advanced Spaceborne Thermal Emission and Reflection Radiometer (ASTER) multispectral data to delineate bauxite deposits over Mainpat plateau, Surguja district, Chhattisgarh, India. Application of specific band combinations help to delineate bauxite in the (SWIR) region (2.16-2.33 µm) and visible near infrared (VNIR) band (0.4–1.0 µm) of multispectral ASTER data. Various image processing techniques like atmospheric correction, minimum noise fraction, pixel purity index, n-dimensional visualiser, and spectral angle mapper were applied to ASTER image to delineate bauxite rich zones. The pure pixels were differentiated from the mixed pixels using pixel purity index which were further subjected to n-dimensional visualiser to identify the target end-members. The presence of bauxite was confirmed by comparing the spectral signatures of end-members with in-built spectral plots of United States Geological Survey spectral libraries and categorized as bauxite and ferruginous bauxite. Finally, the end-members were categorised as bauxite and ferruginous bauxite and mapped using spectral angle mapper. The result obtained was further compared with the lithological map provided by Geological Survey of India for accuracy. Then XRF analysis was carried out for the collected samples to confirm the presence of bauxite and ferruginous bauxite. Geochemical analysis also categorized the samples as bauxite and ferruginous bauxite that added accuracy to the results obtained from remote sensing technique. This study might be considered as a time saving eco-friendly exploitation of natural resources and finally the potential of multispectral ASTER data for mapping mineral resources.**

## INTRODUCTION

Multispectral and hyperspectral satellite data are utilized to distinguish a wide range of rocks and minerals viz. OH bearing minerals, sulphates, carbonates, pyroxenes, olivine, iron oxides and hydroxides (Gupta 2003; Rowan and Mars 2003; Zhang and Pazner 2007; Liu et al. 2011). However, Advanced Spaceborne Thermal Emission and Reflection Radiometer (ASTER) data with the help of specific bands are appropriate for distinguishing such minerals within its spectral range of 0.52-11.65 µm. ASTER data consists of three spectrum bands: visible near infrared (VNIR) with spectral range of 0.52-0.86 µm, short wave infrared (SWIR) with spectral range of 1.6-2.43 vm, and thermal infrared (TIR) with spectral range of 8.125-11.65 µm. Aluminous minerals are distinguished by its high absorbance with in the short wave infrared (SWIR) region (2.16-2.33 µm), iron oxides by absorbance in visible near infrared (VNIR) region (0.4–1.0 ìm), carbonate minerals and OH bearing clay minerals by absorbance in SWIR region (0.9–2.5 Vm) and silica by absorbance in TIR region (8–14 vm) (Bhadra et al. 2013). Bauxite mineral shows significant variation in reflectance at different spectral bands. So with the use of multispectral data like ASTER, it can be effectively mapped (Mujabar and Dajkumar, 2019). The wide spectral range of ASTER data in the VNIR-SWIR region can be used to delineate bauxite within the lateritic deposits. The spectral variations between bauxite and laterite are prominent in the VNIR-SWIR region which can be used for their spectral variations (Aravindan et al. 2020)

India has rich deposits of bauxite. These deposits are fundamentally confined to lateritic regions; as in the case of bauxite deposits at the central eastern part of India. Laterites and bauxites are the resultant of tropical weathering. The power of leaching process and its geochemical composition controlled by Eh and pH of the solvent, which acts as a draining agent during leaching of the parent rock for residual deposit of the mineral decides whether laterite or bauxite will be formed under same environment (Petersen, 1971; Norton, 1973). Outline of the bauxite rich pockets inside the laterites is the essential prerequisite to start review for bauxite investigation. It is difficult to isolate bauxite from laterite in spatial domain utilizing traditional methods as the two minerals are related to one another and are the resultant of same dynamic cycle of chemical weathering of same source rock. Thus, the comparative minerals can be found in both the lithologies yet with differing amounts as well as with a conversion from one form to another by forming transitional products in the outcrop. Generally, bauxite is rich in aluminium hydroxides (gibbsite) and laterite is rich in oxides and hydroxides of iron.

## GEOLOGY OF MAINPAT PLATEAU

Mainpat plateau is situated in Surguja district in the northern part of the state of Chhattisgarh, India. It falls within the survey of India topographic sheet no. 64N/1, 64N/5, and 64N/6. The range is

**Table 1** Stratigraphic succession of Mainpat plateau (after Adil et al. 2013)

| Period | Supergroup/ | Litho-units |
|---|---|---|
| Recent | Group | Bauxite, aluminious laterite, clay. |
| Upper Cretaceous to Lower Paleocene | Deccan Traps | Basaltic lavas. |
| Cretaceous | Lameta | Sandstone |
| Upper Carboniferous to Lower Cretaceous | BarakarTalchir | Coarse to fine grained sand-stone, coal bed, siltstone, green shale. |
| Middle to upper Carboniferous | Gondwanas | Sandstone, conglomerate. |
| Precambrian | Chhattisgarh | Granite-gneiss, phyllite, quartzite etc. |
| Archaean | Basement | Gneiss complex, quartzite, phyllite, acidic to basic intrusions. |

between longitudes E 83°00'00" to 83°25'00" and latitudes N 22°42'50" to 22°55'5". The minimum height of the region is about 810m and maximum height is about 1125m. A variety of rocks like basalt, arkose, shale, syenite, and granite constitute the plateau. These deposits vary in age from Archaean to recent. Deccan traps form the major components at the top and the bottom is composed mostly of gneissic complex, quartzite, and basic intrusions. The bauxite deposit is encountered within the top basaltic layer. Since the plateau has a flat topography, mining practice is carried out easily by different companies like BALCO. Bauxite deposit is present up to a depth of about 9-15m, after which lithomarge (clay layer) is present. Then basalt layer is present after which no bauxite is found. Red/yellow lateritic soil, loamy, and muddy soil are the major soil types. The stratigraphic succession is shown below (Table 1).

**Table 2.** Sampling details

| Sample location no. | Location | Coordinates |
|---|---|---|
| 1 | Asgawan | 83°14'04.11"E 22°50'51.55"N |
| 2 | Sapnadar | 83°15'32.75"E 22°51'42.85"N |
| 3 | Sapnadar | 83°18'16.63"E 22°51'21.48"N |
| 4 | Maltipur | 83°22'35.97"E 22°52'35.58"N |
| 5 | Kuniya | 83°20'26.30"E 22°50'21.63"N |

## GEOLOGY OF THE STUDY AREA

The present study area of Mainpat plateau falls in Surguja district, Chhattisgarh state, India. It is present within the topographic sheet no 64N/5, between longitudes 83°12'0" to 83°23'8.75" E and latitudes 22°49'00" to 22°53'30" N (Fig. 1) covering an area of 83.26 sq. km. The minimum height of the plateau is 855 m and maximum height is 1080 m above MSL. The base map of the study area is given in Fig.1. The sampling details are given in Table 2.

The study area has a variety of mineral deposits belonging to various geological formations (Fig. 2). The major deposits of the study area are bauxite/laterite, basalt, granite gneiss, and sandstone. Bauxite/laterite is formed from the alteration of Deccan basalts belonging to upper Cretaceous to lower Paleocene age. Central India Shear Zone (CISZ) passes through the central region of the plateau trending E-W, which has subjected the area to intense shear and fault. The granite gneiss belongs to the Chhotanagpur gneissic complex, and sandstone belongs to Lower Gondwana. Basalt, granite gneiss, and sandstone are exposed in places where elevation is less than 1000 m, mostly towards the western and eastern regions.

## MATERIALS USED

### Sattelite Data

For image processing, ASTER Level 1T (AST L1T) data is used.

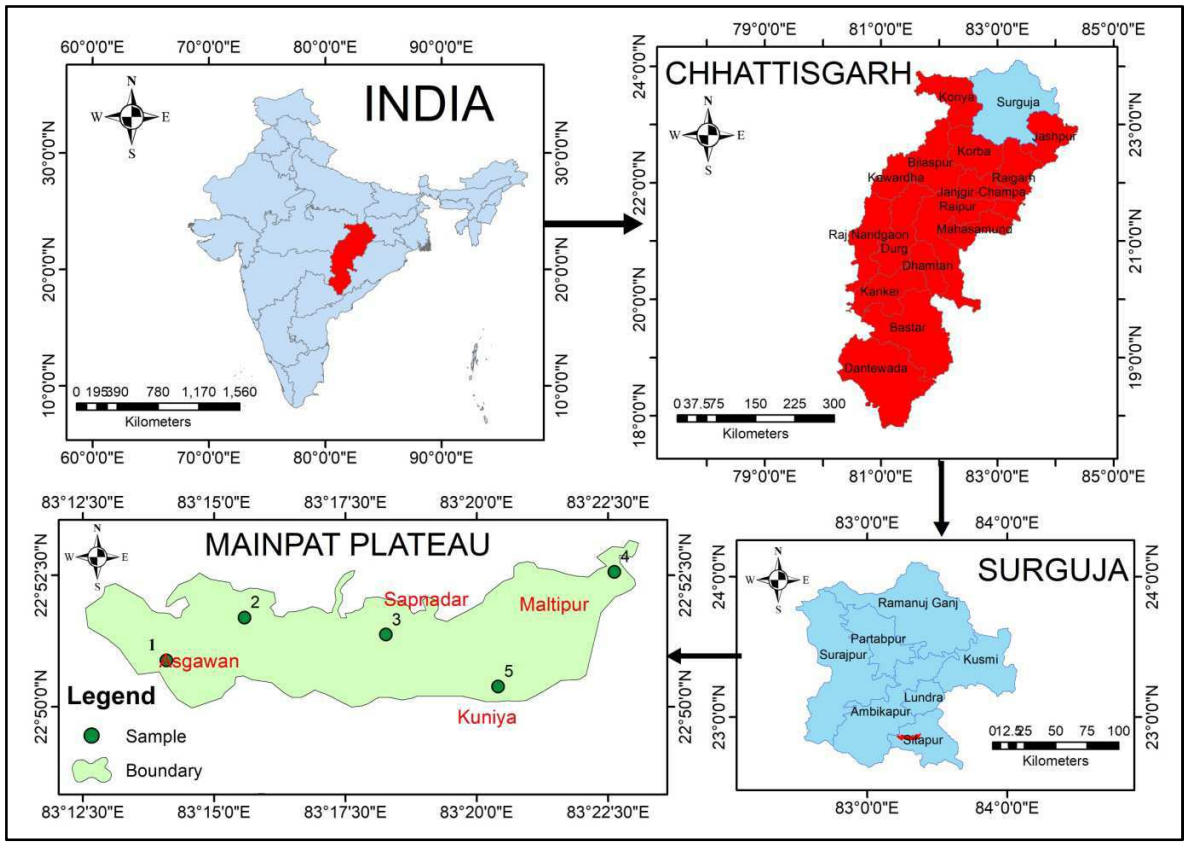


**Fig. 1.** Base map showing the location of the study area and the sampling points.

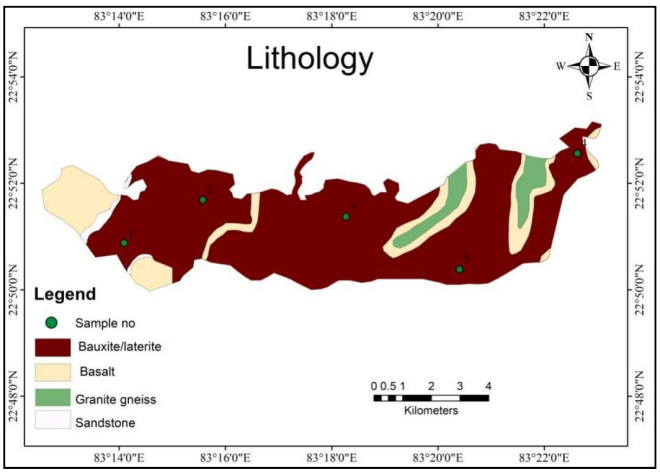


**Fig. 2.** Lithology of the study area

ASTER (Advanced Space borne Thermal Emission and Reflection Radiometer) capture average dataset within 14 bands, between visible to the thermal infrared wavelengths; and furthermore gives stereo viewing digital elevation model (ASTER 2011). Here, nine spectral channels of ASTER data between spectral wavelengths range 0.52 ìm to 2.43 ìm are used. These channels are called ASTER Visible Near Infrared (VNIR) and Short Wave Infrared (SWIR) channels. AST L1T has 'Radiance-At-Sensor' information along with geometric correction already applied to it. ASTER SWIR channels are significant for identifying absorption peaks of minerals with the Al-OH, $CaCO_3$, and Mg-OH, bonds while the ASTER VNIR channel can feature the assimilation highlights of the iron-hydroxides. ASTER sensor is better applicable for delineating economic minerals such as bauxite with the help of spectral signatures compared to other multispectral sensors like SPOT, Landsat and Indian Remote Sensing (IRS) satellites (Zhang et al. 2007). This is because ASTER sensors have six spectral channels where each channel is suitable for specific lithological mapping. Moreover, ASTER inferred digital elevation information can give excellent topographical data appropriate to study the landscape morphology (Abrams 2000) which is additionally important for understanding the geological controls for formation of bauxite.

### Geological Map

The toposheet (unpublished) of the study area of scale 1:50,000 prepared by the Survey of India by means of field mapping along with geological map prepared by Geological Survey of India (https://bhukosh.gsi.gov.in/Bhukosh/MapViewer.aspx) is used as a reference to compare the results obtained from the satellite data. On the basis of remote sensing results, topographic sheets, and interpretation of geological map, an intensive field work was carried to validate the obtained results. It is also significant to study the lithological properties and the parent rock for bauxitization process. Then samples were collected from various parts for geochemical analysis.

### Geochemical Analysis

XRF analysis to obtain the elemental composition of 5 bauxite/laterite samples were carried out at Laboratory of National Institute for Interdisciplinary Science and Technology (NIIST), CSIR, Thiruvanathapuram with the assistance of a Bruker model S4 Pioneer successive wavelength dispersive X-ray spectrometer and equipped with a goniometer, 60 sample programmed loading system, 4 kW Rh X-ray tube, 0.23° and 0.46° collimators. The detector comprises of an argon/methane counter of flow proportion and a scintillation counter. SPECTRA plus software was utilized for the qualitative and quantitative analysis of elements in laterite/bauxite.

## METHODOLOGY

A schematic flowchart is given (Fig. 3) to summarize the method applied over the ASTER L1T data for processing, analyzing, and

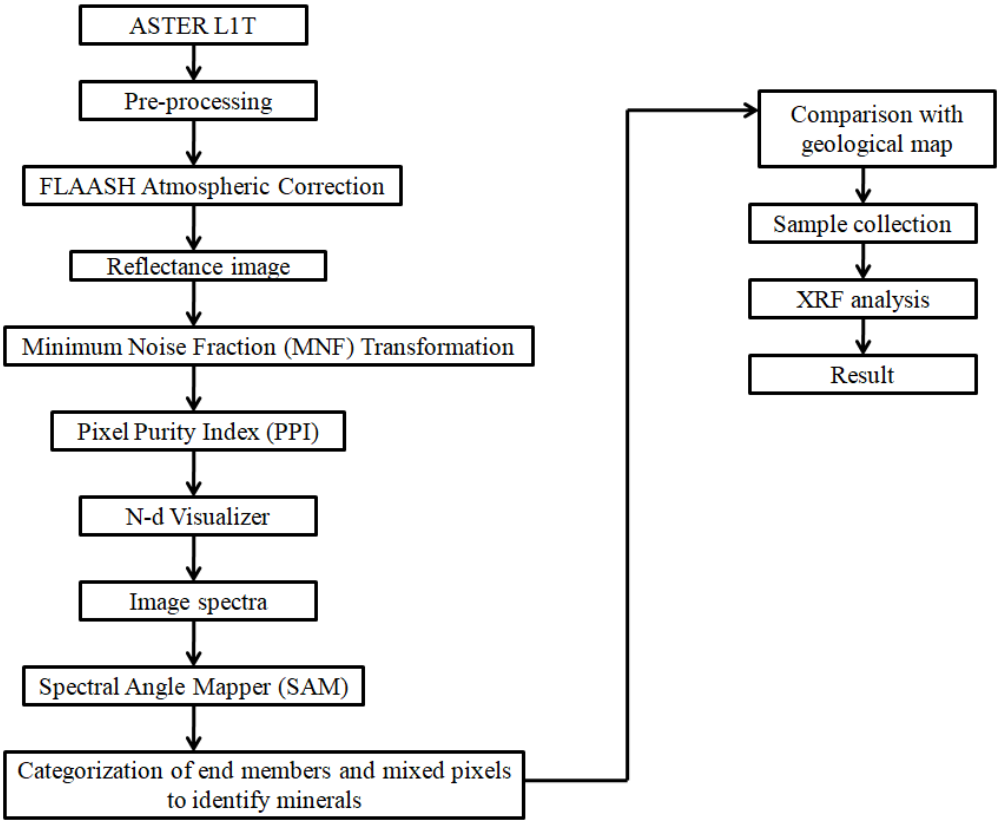


**Fig. 3.** Flow chart showing the methodology adopted.

derivation of bauxite abundant pockets along with the geochemical analysis of the collected samples.

**Pre-processing ASTER Data**

The ASTER data is first pre-processed to get the reflectance image. Out of the 14 spectral bands present in the ASTER L1T data, three bands belong to VNIR spectrum (Band 1 to Band 3), six bands belong to SWIR spectrum (Band 4 to Band 9) and five bands (band 10 to 14) belong to TIR spectrum. For bauxite delineation, nine bands (Band 1 to Band 9) within the spectral region of VNIR and SWIR are used. These spectra are separated on the basis of their spatial resolution. For the purpose of bauxite delineation, first the nine spectral bands of the terrain revised L1T data have been stacked to a single layer in order to further process by using the ENVI 4.7 software programmed layer stacking tool. The layer stacked image is in Band Sequential (BSQ) format and it has to be converted to Band Interleaved by Line (BIL) format. After this, the layer stacked image is subjected to Radiometric Calibration. The data is processed to eliminate the atmospheric noises due to the presence of water vapour, dust particles, clouds etc in the satellite image by utilizing the atmospheric correction tool "Fast Line-of-sight Atmospheric Analysis of Spectral Hypercubes (FLAASH atmospheric correction)" (Matthew et al. 2000). The FLAASH model is calibrated by entering the details of the ASTER image like sensor and scene information, altitude of sensor, elevation from ground, latitude and longitude derived from the scene centre location, time of flight GMT, date of flight, atmospheric model, aerosol model etc. These data are gathered from the ASTER.HDF file metadata. The calibration of the reflectance data is performed with prelaunch gains and offsets determined for ASTER sensors. After getting reasonable calibration parameters of the ASTER data, the model removes the atmospheric effects and recovers the spectral reflectance from the multispectral radiance image. After applying the atmospheric correction, the digital number (DN) of the image reveals the original features of the terrain as a reflectance data (Fig. 4).

The nature of the final reflectance image is estimated by comparing the image spectra of different pixels of land, water and vegetation and its ASTER convolved lab spectra. After acquiring the clear reflectance image, it is exposed to the ENVI hourglass spectral analysis which follows the different steps of ASTER data processing.

**ASTER Data Processing**

Minimum noise fraction (MNF) transformation is used to establish the inherent dimensionality of the image content, isolate noise in the data, and decrease the computational requisites for further processing (Boardman and Kruse 1994). Chen (2000) states the advantages of MNF transformation over the Principal Component Analysis to reduce the dimension of hyper-spectral image. MNF is a linear transformation, implemented in ENVI and follows a separate principal component analysis rotation. The first rotation is called 'noise whitening' where principal components of the noise covariance matrix are used to decorrelate and rescale the noise in the data. As a result principal components are derived from the original image data which have been noise-whitened and the second rotation uses these components. In second rotation, the derived principal components are rescaled with the use of noise standard deviation. In this study, the MNF is applied

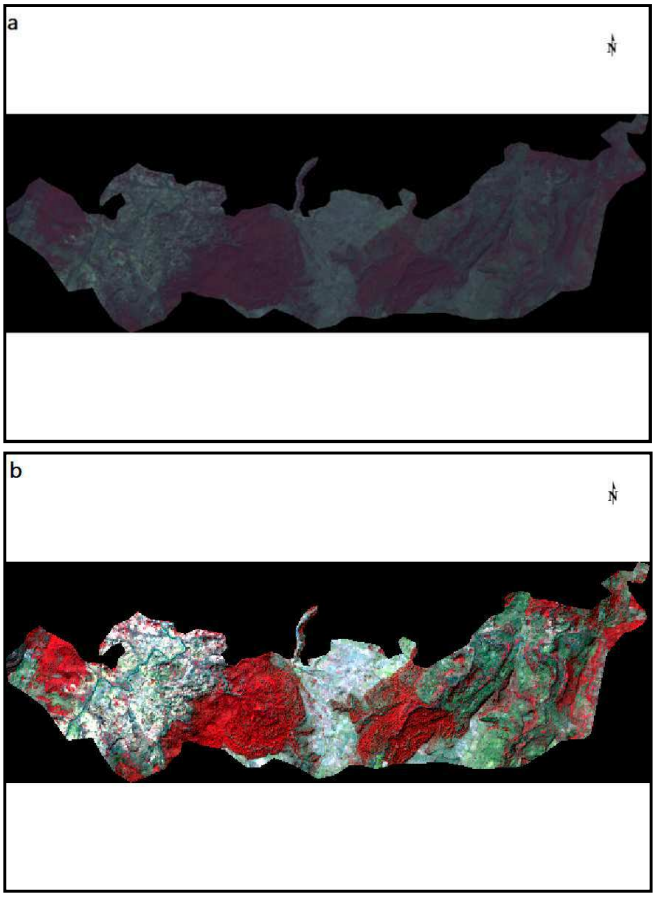


**Fig. 4.** False colour composite (FCC) of the study area with band combination 3, 2, 1 (3- Red, 2- Green, 1- Blue). **(a)** Shows ASTER L1T image before atmospheric correction and **(b)** After atmospheric correction

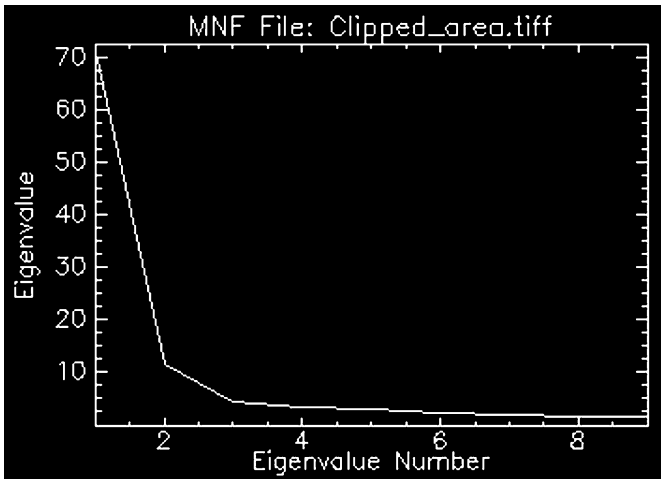


**Fig. 5.** Plot showing Eigen Number and Eigenvalue for different MNF bands.

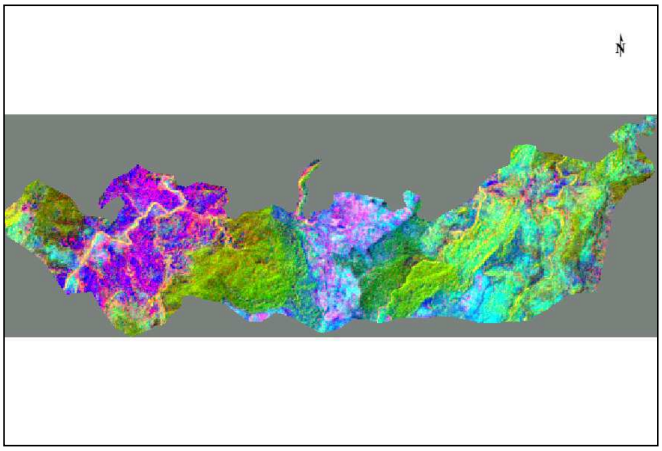

**Fig. 6.** Showing the resultant MNF forward rotation with RGB band combination (3, 2, 1).

to the atmospheric corrected ASTER data and it creates nine MNF transformed bands which can be seen and further analyzed. Figure 5 shows the MNF plot of Eigen values comparing to various MNF bands or Eigen number. Figure 6 shows the RGB image of the MNF bands 3, 2 and 1, which are useful in distinguishing the target end-member spectra along with structural features passively amplified as fold, with vegetation.

The resultant output band of MNF is processed and the pure pixels are derived. This derivation is achieved from the variance level derived from band 1, 2, 3, 4, 5, 7, and 8 (Balasubramanian et al. 2012). Then their noise is reduced for further processing and delineation of pure pixels from mixed pixels was carried out. This was achieved using Pixel Purity Index (PPI) keeping the threshold value at 0.8 with 10,000 iterations. With this threshold value and iterations, 4,000 pixels were selected as pure pixels (Fig. 7).

The pure pixels was further analysed to delineate the purest pixels and categorize into region of interest (ROI) which was derived for the mineral identified by maximum score values. For this, n-Dimensional visualisation was carried out on the end member spectra (Fig. 8) and the result was correlated, through spectral analysis, with the United States Geological Survey (USGS) inbuilt spectral library.

The spectra of bauxite is studied with reference to the spectral signature of gibbsite (main constituent mineral of bauxite) based on the USGS spectral library (Fig. 9). These spectra and the resultant spectra of ASTER image (Fig. 10) was compared for identification of bauxite. The comparative analysis is used to differentiate bauxite and ferruginous bauxite on the basis of their dominance in bauxite or laterite respectively (Guha et al., 2013). The resultant spectral signature of

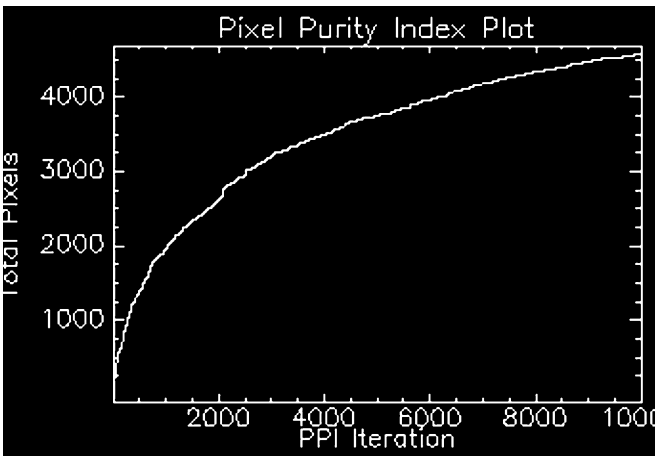


**Fig. 7.** PPI plot.

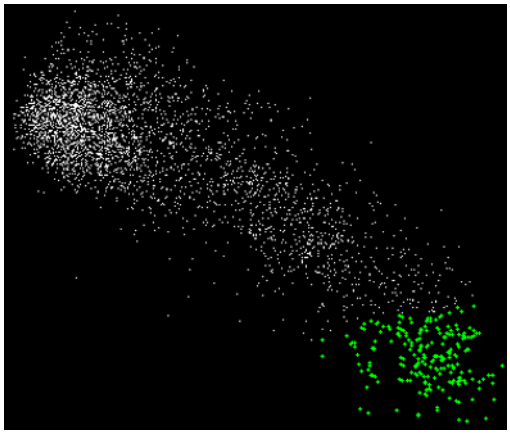

**Fig. 8.** n-dimensional visualization showing cluster of endmembers. Purest pixels (green colour) at the edges show spectral signatures of bauxite.

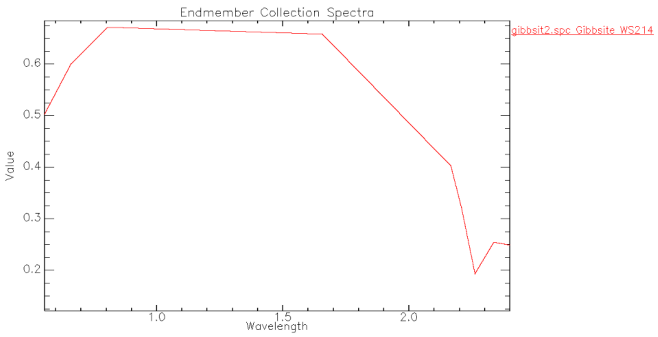


**Fig. 9.** Spectra of gibbsite (ASTER derived) in USGS library.

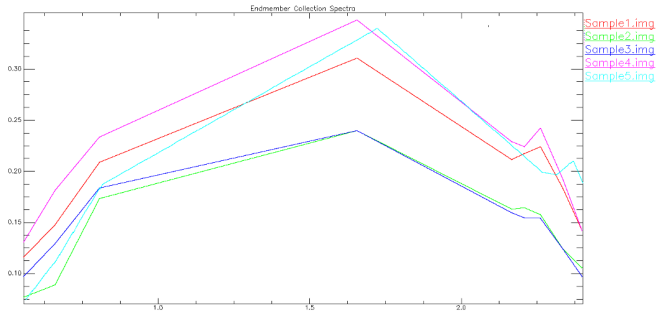


**Fig. 10** ASTER convolved image spectra categorizing bauxite and ferruginous bauxite on the basis of dominancy of bauxite and laterite respectively.

sample-5 showed an absorption dip at 2.26 ìm, inferring it to be bauxite. The result was further confirmed with geochemical analysis. The end-members showed maximum score for lateritic bauxite. Therefore, they were categorised on the basis of their maximum scores towards the corresponding spectral library in the region of interest.

Then to the categorised end-member, region of interest is applied on the VNIR-SWIR bands of ASTER data using spectral angle mapper (SAM). SAM is a process used to determine the similarity between a pixel and the reference spectra on the basis of calculation of 'spectral angle' between them (Boardman and Kruse 1994). SAM considers both the known and unknown spectra as vectors and estimates the spectral angle between them as shown in Fig. 11. The spectral angle for identification of bauxite is set to 0.2°. On applying SAM over the 9 band data of ASTER L1T (Crosta and De Souza Filho 2000; Das

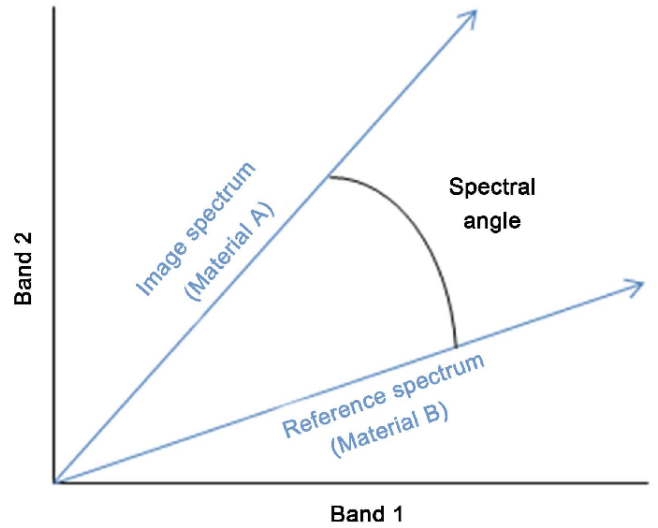


**Fig. 11.** Algorithm of spectral angle mapper algorithm (Hamza et al. 2016)

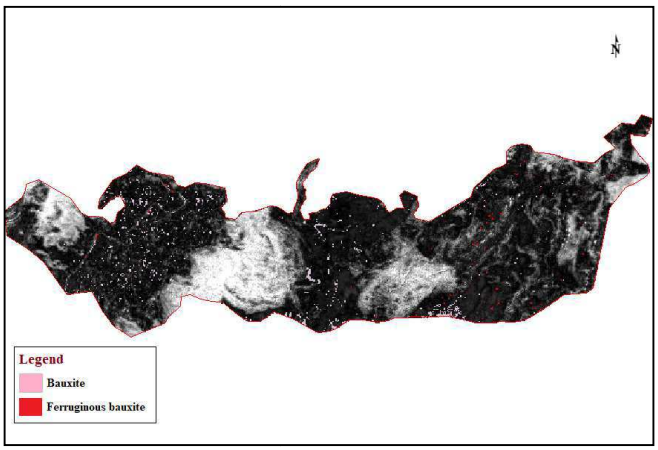


**Fig. 12.** SAM classified image showing bauxite and ferruginous bauxite

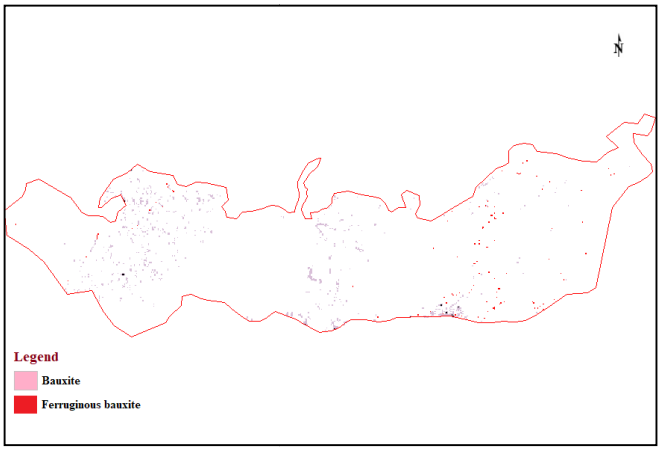


**Fig. 13.** Final output map showing bauxite and ferruginous bauxite.

2002; Crosta et al. 2003; Kruse and Perry 2006; Gersman et al. 2007), the pixels of the identified minerals are shown on the classified image. After defining the ROIs of the corresponding minerals, the bauxite abundant pockets over the study area is mapped as shown in Fig 12. Bauxite and ferruginous bauxite are represented in pink and red colour respectively. The brighter tone (white colour) represents forest area.

The resultant SAM image was compared with the geological map and it gave well defined accuracy. In Fig. 12, bauxite is detected through remote sensing technique in areas where they are exposed on the surface whereas in the geological map (Fig. 2), major portion of the area is occupied by bauxite deposits. This variation might have occurred due to the presence of thick forest that restricted ASTER image to penetrate through it. It was observed that some of the bauxite deposits were located in the slope as well as low lying regions which might have caused due to erosion and stream depositions. So the final map is extracted from elevations greater than 900 m to remove the errors caused by the slopes as shown in Fig. 13.

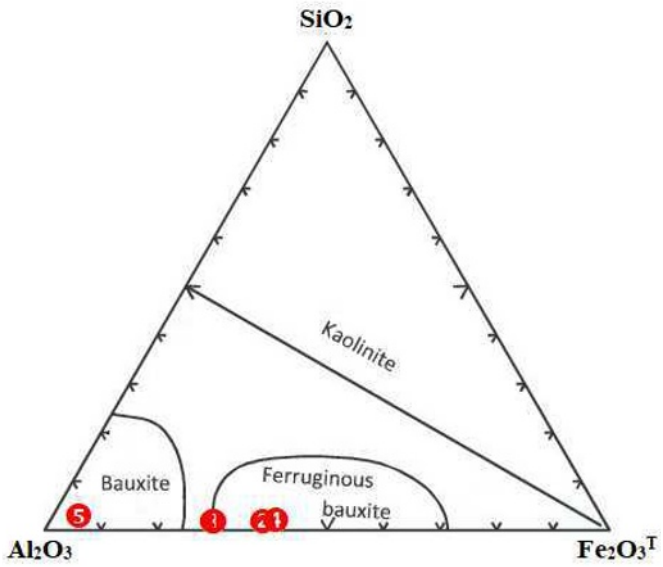


**Fig. 14.** Chemical classification of Mainpat bauxite deposits after Aleva (1981).

## GEOCHEMISTRY OF BAUXITE

X – ray fluorometry analysis of bauxite was done to study the geochemistry of the samples more precisely. It showed remarkable variations in composition with respect to major and trace elements. The major elements observed in the collected samples in weight % are shown in Table 3. The weight % of major elements like $SiO_2$, $Al_2O_3$, $Fe_2O_3$, and $TiO_2$ ranges from 0.79-1.80, 52.17-75.31, 3.53-28.94, and 10.12-14.46 respectively.

In Fig. 14, most of the samples fall in the ferruginous bauxite zone, implying to be laterites whereas some samples fall in the bauxite zone, implying to be bauxites (Boulange et al. 1996). Therefore, the deposits of Mainpat could be classified as bauxite and ferruginous bauxite.

## RESULT AND CONCLUSION

With the comparative study of multispectral data, geological map, and field work, the final bauxite abundance map was derived. In this current investigation, the utilization of multispectral ASTER data for bauxite mineral mapping has been illustrated. Multispectral data covering the study area was analysed with the help of various image processing techniques which had demonstrated its potential in identification of bauxite deposits. The classified image showed the abundance of bauxite mineral along the investigation area. Minor variation of bauxite abundance between ASTER image and geological map was observed which is due to presence of thick forest (red colour of FCC image in Fig 4 b) in the area. The bauxite mineral showed wide variation in reflectance at various spectral bands and was effectively mapped with the use of multispectral data. The mineral resource was classified with the use of SAM per-pixel method. The multispectral data was very useful to identify and locate the bauxite

**Table 3.** Major element composition of bauxite samples

| Sample no | $Al_2O_3$ | $SiO_2$ | $P_2O_5$ | CaO | $TiO_2$ | MnO | $Fe_2O_3$ | MgO | $Na_2O$ | $K_2O$ |
|---|---|---|---|---|---|---|---|---|---|---|
| 1 | 65.36 | 1.052 | 0.3109 | 0.0059 | 10.12 | 0.014 | 22.910 | 0.0028 | 0.028 | 0.0020 |
| 2 | 52.171 | 0.872 | 0.591 | 0.261 | 14.461 | 0.046 | 26.357 | 0.0029 | 0.013 | 0.0079 |
| 3 | 53.09 | 0.798 | 0.891 | 0.051 | 12.375 | 0.039 | 18.293 | 0.0030 | 0.011 | 0.0012 |
| 4 | 52.81 | 1.091 | 0.510 | 0.702 | 13.25 | 0.042 | 28.944 | 0.0030 | 0.013 | 0.0015 |
| 5 | 75.315 | 1.801 | 0.481 | 0.21 | 10.60 | 0.028 | 3.539 | 0.0027 | 0.01 | 0.0730 |

abundant pockets which could lead to eco-friendly and sustainable exploitation of the mineral resource along the region. The attempt of the study brought out the use of the wide spectral data of ASTER image in the visible-near infrared and short wave infrared (VNIR-SWIR) region for delineating bauxite and ferruginous bauxite. The spectral contrast between the bauxite and ferruginous bauxite could be differentiated in the VNIR-SWIR region. The image spectra derived from ASTER image was compared with the spectra of gibbsite (from USGS library) and categorised as bauxite and ferruginous bauxite on the basis of their dominancy in bauxite and laterite respectively. As a result these contrasts were used to generate ASTER based SAM images for their separation. Geochemical analysis of the samples supported the presence of bauxite over the study area. The samples collected could be categorised as bauxite and ferruginous bauxite.

*Acknowledgements:* Authors are thankful to Dept of Earth Sciences, Annamalai University, Tamil Nadu for setting a platform on research activities. We are pleased to thank Dr Sundararajan M., Principal Scientist CSIR-NIIST, Thiruvananthapuram, Kerala for helping to carry XRF analysis.

**References**

Abrams, M. (2000) The Advanced Spaceborne Thermal Emission and Reflection Radiometer (ASTER): data products for the high spatial resolution imager on NASA's Terra platform. Internat. Jour. Remote Sensing, v.21(5), pp.847–859.

Adil, S.H., Patel, V.N., Trivedi, R.K., Gupta, S.K., Golekar, R.B. (2013) Structural evolution of Mainpat plateau, Surguja district, Central India. https ://cites eerx.ist.psu.edu/viewdoc/download?doi=1 0.1.1.975.3122& rep=rep1&type=pdf

Aravindan, S., Bharathiraja, S. and Sanjay Kumar Balabantaray (2020) Hyper spectral signature and ASTER data analysis for mapping of Bauxite deposits in Shevaroy hill of Tamil Nadu, India. Internat. Res. Jour. Earth Sci., v.8(1), pp.13-19. http://www.isca.me/EARTH_SCI/Archive/v8/i1/3.ISCA-IRJES-2019-015.pdf

ASTER. http://en.wikipedia.org/wiki/Advanced Spaceborne Thermal Emission and Reflection Radiometer (Date of refer: 10-08-2011).

ASTER-GDEM: www.jspacesystems.or.jp/ersdac/GDEM/E/ (Date of refer: 13-10- 2011).

Balasubramanian, U.R., Saravanavel, J., Gunasekaran, S. (2012). Ore mineral discrimination using hyperspectral remote sensing—a field-based spectral analysis. Arabian Jour. Geosci., v.6(12), pp.4709-4716.

Bhadra, B.K., Pathak, S., Karunakar, G. and Sharma, J.R. (2013) ASTER data analysis for mineral potential mapping around Sawar-Malpura area, Central Rajasthan. Jour. Indian Soc. Remote Sensing, v.41(2), pp.391-404.

Boardman, J.W. and Kruse, F.A. (1994) Automatic Spectral Analysis: A Geological Example Using AVIRIS Data, North Grapevine Mountain, Nevada. *In:* 10th Thematic Conference on Geologic Remote Sensing, Ann Arbor, pp.407-418.

Boulange, B., Bouzat, G., Pouliquen, M. (1996) Mineralogical and geochemical characteristics of two bauxitic profiles, Fria, Guinea Republic. Mineralium Deposita, v.31, pp.432–438.

Chen, C.M. (2000) Comparison of Principal Components Analysis and Minimum Noise Fraction Transformation for Reducing the Dimensionality of Hyper-Spectral Imagery. Geographical Res., v.33(2), pp.163–178.

Crosta, A.P. and De Souza Filho, C.R. (2000) Hyperspectral remote sensing for mineral mapping: a case-study at Alto Paraíso De Goías, Central Brazil. Revista Brasileira de Geociências, v.30(3), pp.551–554.

Crosta, A.P., De Souza, C.R., Azevedo, F., Brodie, C. (2003) Targeting key alteration minerals in epithermal deposits in Patagonia, Argentina, using ASTER imagery and principal component analysis. Internat. Jour. Remote Sens., v.24(21), pp.4233–4240.

Das, I.C. (2002) Spectral signatures and spectral mixture modeling as a tool for targeting aluminous laterite and bauxite ore deposits. GIS development.net, Koraput, India

Gersman, R., Ben Dor, E., Beyth, M., Avigad, D., Abraha, M., Kibreab, A. (2007) Hyperspectral remote sensing as a tool for geological exploration—examples from the Northern Danakil Depression, Eritrea. Proc. 5th EARSeL Workshop on Imaging Spectroscopy. Bruges, Belgium, April 23–25, 2007, pp.1–14.

Guha, A., Singh, V.K., Parvee, R., Kumar, K.V., Jeyaseelan, A.T. Dhanamjaya Rao, E.N. (2013) Analysis of ASTER data for mapping bauxite rich pockets within high altitude lateritic bauxite, Jharkhand, India. Internat. Jour. Appl. Earth Obs. Geoinf., v.21, pp.184–194.

Gupta, R.P. (2003) Remote Sensing Geology, 2nd Edition. Springer-Verlag: berlin, Heidelberg, New York, 656p.

Hamza, M.H., Al Thubaiti, A.S., Dhieb, M., Ali, A.B.H., Garbouj, M.S. and Ajmi, M. (2016). Dasymetric mapping as a tool to assess the spatial distribution of population in Jeddah City (Kingdom of Saudi Arabia). Current Urban Studies, v.4(3), pp.329-342.

https://bhukosh.gsi.gov.in/Bhukosh/MapViewer.aspx

Kruse, F.A., Perry, S.L. (2006) Regional mineral mapping by extending hyperspectral signatures using multispectral data. IEEEAC paper #1078, version 4, updated November 24, 2006. pp: 1–15.

Liu, L., Zhuang, D., Zhou, J. and Qiu, D. (2011) Alteration mineral mapping using masking and Crosta technique for mineral exploration in mid-vegetated areas: A case study in Areletuobie, Xinjiang (China). Internat. Jour. Remote Sensing, v.32(7), pp.1931–1944.

Matthew, M.W., Adler-Golden, S.M., Berk, A., Richtsmeier, S.C., Levine, R.Y., Bernstein, L.S., Ratkowski, A.J. (2000) Status of atmospheric correction using a MODTRAN4-based algorithm. In Algorithms for multispectral, hyperspectral, and ultraspectral imagery VI (Vol. 4049, pp. 199-207). International Society for Optics and Photonics.

Norton, S.A. (1973) Laterite and bauxite formation. Econ. Geol., v.68(3), pp.353-361.

Petersen, U. (1971) Laterite and bauxite formation. Econ. Geol., v.66(7), pp.1070-1071.

Rowan, L.C. and Mars .JC. (2003) Lithologic mapping in the Mountain Pass, California area using Advanced Spaceborne Thermal Emission and Reflection Radiometer (ASTER) data. Remote Sensing and Environ., v.84, pp.350–366.

Sheik Mujabar, P. and Dajkumar, S. (2019) Mapping of bauxite mineral deposits in the northern region of Saudi Arabia by using Advanced Spaceborne Thermal Emission and Reflection Radiometer satellite data. Geo-spatial Information Sci., v.22(1), pp.35-44. DOI:10.1080/10095020.2018.1530857

Zhang, X. and Pazner, M. (2007) Comparison of lithologic mapping with ASTER, Hyperion, and ETM Data in the Southeastern Chocolate Mountains, USA. Photogrammetric Engineering & Remote Sensing, v.73(5), pp.555–561.

Zhang, X., Pazner, M. and Duke, N. (2007) Lithologic and mineral information extraction for gold exploration using ASTER data in the south Chocolate Mountains (California). ISPRS Jour. Photogrammetry and Remote Sensing, v.62, pp.271–282.